LANGMUIR

pubs.acs.org/Langmuir Article

Head-on Collision of Two Nanodroplets on a Solid Surface: A Molecular Dynamics Simulation Study

Peng Mao, Shan Gao, Wei Liu,* and Zhichun Liu*

Cite This: *Langmuir* 2021, 37, 12346−12355 Read Online

ACCESS | Metrics & More | Article Recommendations | Supporting Information

ABSTRACT: Most researchers focus on the collision of a single droplet with a solid surface, while it is common for a droplet to collide with a sessile droplet on a solid surface in reality. This study performed the head-on collision of two nanodroplets on a solid surface using the molecular dynamics simulation method. The effects of impact velocity, interaction intensity between solid and liquid atoms, and the solid fraction of the surface on the collision process are studied with independent simulation cases. The maximum spreading factor and the dimensionless maximum spreading time are recorded and calculated to describe the collision process quantitatively. The simulation results indicate that the maximum spreading factor depends more on the solid fraction than the interaction intensity since it does not fundamentally change the wetting state of the droplet at its maximum spreading state. Because of two different effects, the maximum dimensionless spreading time decreases first and then increases with the interaction intensity, and both effects weaken with the increase of impact velocity. As the solid fraction increases, the maximum spreading factor increases significantly at high impact velocity, and the maximum dimensionless spreading time first decreases and then increases because the wetting state of the coalescent droplet at the maximum spreading moment gradually changes from the Wenzel state to the Cassie state. In general, the initial wetting state of the sessile droplet and the wetting state of the coalescent droplet at the maximum spreading moment have important effects on the maximum spreading factor and the maximum spreading time. We establish a theoretical prediction model for the maximum spreading factor on a smooth surface based on energy conservation with quite good accuracy. This research has improved our understanding of the head-on collision process of two nanodroplets on a solid surface.

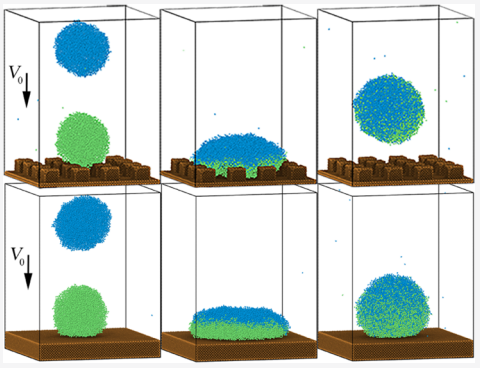

INTRODUCTION

The collision of droplets is a ubiquitous phenomenon in nature and industrial applications. It is of great significance to explore and understand the rules and influencing factors of the droplet collision process for the development of surface self-cleaning,[1−6] inkjet printing,[7] enhanced droplet condensation,[8] and anti-icing.[9−11] At present, researchers are very concerned about the collision process between droplets and a solid surface at the micro/nanoscale. In general, there are two research lines to study droplet collision.

For a droplet colliding with the solid surface, a wide range of experiments[12−20] and simulations[21−27] show that the roughness and the wettability of the surface have an important influence on the spreading and retraction of colliding droplets. The colliding droplets show a variety of interesting scenarios, including deposition, prompt splash, coronal splash, receding breakup, partial rebound, and complete rebound. The parameters used in the literature to describe the collision process include the maximum spreading factor β_{max} ($\beta_{max} = D_{max}/D_0$, where D_{max} denotes the maximum spreading diameter and D_0 denotes the initial diameter), the maximum spreading time τ_{max} (the time from the start of collision to the maximum spreading state), the Weber number ($We = \rho D_0 V_0^2/\sigma$), and the Reynolds number ($Re = \rho D_0 V_0/\mu$). Some theoretical models[17−19,28,29] were given to predict β_{max} using energy conservation at the macroscale. Because of the time and space scale limitations involved, it is difficult to conduct research through routine experiments due to problems related to nanodroplets, and the molecular dynamics simulation method has attracted the attention of researchers.[26,27,30−32] Li et al.[33,34] investigated the collision of an Ar nanodroplet with the smooth surface and analyzed the mechanism of breakup in the nanoscale using the MD simulation method, and a theoretical model of the maximum spreading factor was given to improve accuracy for nanodroplets. Gao et al.[35] studied the dynamic behavior of a nanodroplet colliding with rough surfaces, which had various physicochemical properties and revised the previous model. Their models have a good

Received: July 12, 2021
Revised: October 4, 2021
Published: October 14, 2021

https://doi.org/10.1021/acs.langmuir.1c01849
Langmuir 2021, 37, 12346−12355

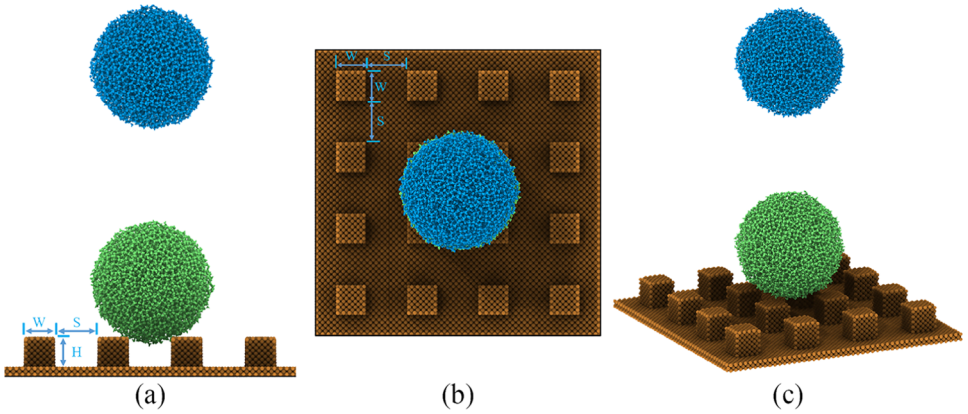

Figure 1. Initial model used in the simulation: (a) front view, (b) top view, and (c) oblique view. To distinguish between different atom types, copper-like atoms are in brown, atoms of the upper droplet are in blue, and atoms of the lower droplet are in green.

match with the simulation results. Therefore, it is believed that the molecular dynamics simulation is a powerful and effective method for studying the collision process of nanodroplets.

The droplets colliding with another liquid body such as a droplet, bath, or film is another research line. Rayleigh pioneered the work, which reported a collision between two droplet streams.[36] For collisions between double droplets, the impact parameter $B = X/R$ is an important factor in collision behavior, where X is the distance between the centroid of two droplets in the direction perpendicular to the relative velocity and R is the droplet radius. Wang et al.[37] conducted an experimental study on the head-on collision of one droplet with another sessile droplet on the PDMS substrate, which shows four different phenomena. Head-on collision means that the impact parameter B is equal to 0. Graham et al.[38] investigated the off-center collision process of two droplets on a solid surface by both experimental and numerical methods and gave a model to predict the maximum spreading length. For the collision process of nanodroplets, it is unclear whether macro phenomena exist and whether the previous theoretical models are applicable, which needs further study.

In this work, we consider the cases where a water nanodroplet collides with another sessile water nanodroplet on a solid surface with various properties. Compared with the collision of a single droplet directly with the wall, the situation studied in this paper is more common because droplets generally tend to appear together in a group. However, there are relatively few studies on the nanoscale two droplet collisions. This study will help us find the mechanism of collision between multiple nanodroplets and the solid wall and provide theoretical guidance for the development of nano-inkjet printing and other technologies. Some parameters were recorded and calculated to describe the collision process, including the dimensionless maximum spreading time τ^*_{max} and the maximum spreading factor β_{max}. Our study on the collision of two nanodroplets is divided into two parts to analyze the effects of different factors. One is to study the effect of impact velocities by keeping the surface fixed. The other is to study the effect of surface properties including the interaction intensity and the solid fraction. In addition, we provide a prediction model of the maximum spreading factor based on energy conservation. The values calculated by this model are in good agreement with the values obtained from the simulation, especially in the range of high impact velocities.

MODELS AND METHODS

All simulations were performed by the large-scale atomic/molecular massively parallel simulator package(LAMMPS)[39] and visualized by the Open Visualization Tool (OVITO).[40] The simulation system consists of two equal-sized spherical droplets composed of water molecules and a solid substrate composed of copper-like atoms. Both water molecules and copper-like atoms are arranged by a face-centered cubic structure to initialize the physical model. In the simulations of this paper, the system temperature is set to 298 K. The main physical parameters of the droplet at this temperature include the mass density ρ = 997.07 kg/m^3, surface tension σ = 71.99 mN/m, and viscosity coefficient μ = 0.8937 mPa·s.

Physical Model. To investigate the collision process of two nanodroplets on the solid substrate, this paper constructs the physical model shown in Figure 1. The size of the simulation box is 174 Å × 174 Å × 230 Å. Two droplets with a diameter of approximately 75.8 Å consist of 15 226 water molecules in total. Different rough surfaces are constructed by changing the square column structure size parameters, including the square column length W, spacing side length S, and square column height H. The specific values of the parameters of different surfaces used in this study are shown in Table 1. The calculation formula of the solid fraction is $\phi_s = W^2/(W + S)^2$.

Table 1. Physical Parameters of Different Models

model	1	2	3	4	5
W (Å)	18.08	21.69	25.31	28.92	
S (Å)	25.31	21.69	18.08	14.46	
H (Å)	18.08	18.08	18.08	18.08	
ϕ_s (%)	17.36	25	34.03	44.44	100

Simulation Details. In this paper, the TIP4P model is used to describe water molecules in the MD simulation. The model's interaction sites include one oxygen atom, two hydrogen atoms, and a massless virtual charge point. The specific parameters of the model are shown in Table 2. Through this model, the potential function between water molecules can be expressed as

$$U_{ij} = 4\varepsilon_{OO}\left[\left(\frac{\sigma_{OO}}{r_{ia,jb}}\right)^{12} - \left(\frac{\sigma_{OO}}{r_{ia,jb}}\right)^{6}\right]_{a=1,b=1} + \sum_{a=1}^{3}\sum_{b=1}^{3}\frac{q_{ia}q_{ib}}{4\pi\varepsilon_0}\frac{1}{r_{ia,jb}} \quad (1)$$

In this formula, the first term is van der Waals interaction represented by the 12-6 type LJ (Lennard-Jones) potential function, the second term is the long-range Coulomb interaction described by the Coulomb potential function, i and j denote different water molecules, a and b denote different sites of interaction in a water molecule, 1 represents the oxygen atom, 2 represents the hydrogen

https://doi.org/10.1021/acs.langmuir.1c01849
Langmuir 2021, 37, 12346−12355

Table 2. Parameters of the TIP4P Model[a]

	q_H (e)	q_O (e)	q_M (e)	ε (kJ/mol)	σ (Å)	r_{OH} (Å)	r_{OM} (Å)	θ_{HOH} (deg)
TIP4P	+0.5242	0.0	−1.0484	0.6813	3.16435	0.9572	0.125	104.52

[a] q_H—charge on the hydrogen atom; q_O—charge on the oxygen atom; q_M—charge on the virtual point; ε,σ—Lennard-Jones parameters; r_{OH}—OH bond length; r_{OM}—the distance of the virtual point from the oxygen atom; and θ_{HOH}—HOH bond angle.

atom, 3 represents the virtual point, ε_{OO} denotes the interaction energy well depth, σ_{OO} denotes the distance where the value of the LJ potential is equal to zero, and ε_0 denotes the vacuum permittivity. In the TIP4P model, only van der Waals interaction between oxygen atoms participates in the calculation, and the stretching and bending bonded interactions are represented by the harmonic style.

The embedded-atom method (EAM) potential is used to calculate the interaction between copper-like atoms in the solid substrate. Substrates with different hydrophilic and hydrophobic properties are generated by changing the potential function parameter ε_{S-O}, which is calculated by the following Lorentz−Berthelot mixing rules

$$\varepsilon_{ij} = \sqrt{\varepsilon_i \varepsilon_j} \tag{2}$$

$$\sigma_{ij} = (\sigma_i + \sigma_j)/2 \tag{3}$$

where i and j denote different atom types. Between copper-like atoms and oxygen atoms, there is only van der Waals interaction, which is represented using the 12-6 type LJ potential function. The interaction intensity f is defined as the ratio between solid−water and water−water potential coefficients

$$f = \varepsilon_{S-O}/\varepsilon_{O-O} \tag{4}$$

The small value of ε_{S-O} allows the solid surface composed of copper-like atoms to exhibit a lower surface energy characteristic, which in turn gives the droplet a large contact angle on the solid surface.

In simulations, periodic boundary conditions are used in the horizontal direction of the simulation box, while fixed conditions and mirror reflection conditions are applied simultaneously to the upper and lower boundaries of the vertical direction. Newton's equation of motion is solved by the velocity Verlet algorithm with a time step of 1.0 fs. A cutoff distance of 10 Å is used in the calculation of van der Waals interaction, and the long-range Coulomb interaction is calculated by the particle−particle−particle−mesh (PPPM) method with a Coulombic cutoff distance of 12 Å. The SHAKE algorithm is used to keep the hydrogen−oxygen bond length and the hydrogen−oxygen−hydrogen bond angle in water molecules fixed.

To reduce the time of calculation, the droplets were initialized into a spherical shape. The entire simulation process can be divided into two steps: (1) The first step is to bring the simulation system into equilibrium. Specifically, two spherical droplets are maintained at 298 K in the NVT ensemble with a Nosé−Hoover thermostat, and the solid substrate is also maintained at 298 K with the NVE ensemble and a Langevin thermostat. (2) In the second step, after the system reaches equilibrium, the Nosé−Hoover thermostat is removed, and the NVE ensemble is used for the total system. The upper droplet is given a downward centroid velocity, which causes the two droplets to collide.

RESULTS AND DISCUSSION

Model Verification. The density and the radial distribution functions, g(O−O), g(O−H), and g(H−H) of a pure water system are calculated and compared with experimental data to verify the model parameters used in the simulation and the correctness of program settings. The verification simulation is performed with a cubic simulation box that applies periodic boundary conditions in each dimension. The system is controlled to a temperature of 298 K and a pressure of 1 atm with the NPT ensemble.

The calculated density of this pure water system is about 0.9898 g/cm^3, while the experimental density of water at 298 K and 1 atm is about 0.9970 g/cm^3, with an error of about 0.72%. As shown in Figure 2, the radial distribution function values

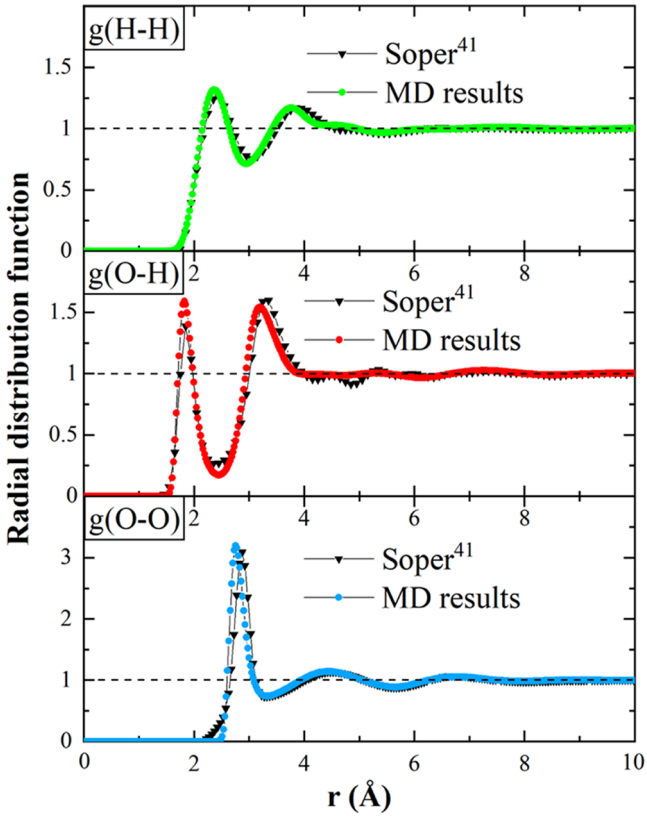

Figure 2. Radial distribution functions g(O−O), g(O−H), and g(H−H) of water. O denotes the oxygen atom and H denotes the hydrogen atom.

calculated in this paper are in good agreement with the experimental values of Soper et al.[41,42] These results indicate that the model parameters and simulation process program settings adopted in this paper are relatively reliable. This lays the foundation for our follow-up research.

Effects of Velocity on the Two Droplet Collision Process. By varying the impact velocities, we establish five independent cases to study the effects of different velocities on the collision process. The details are shown in Table 3, including the impact velocity, the Reynolds number Re, and the Weber number We. All five cases have the same model and

Table 3. Dimensionless Parameters Corresponding to Different Impact Velocities

V_0 (Å/ps)	3	4	5	6	7
Re	2.54	3.38	4.23	5.07	5.92
We	9.45	16.80	26.25	37.79	51.44

https://doi.org/10.1021/acs.langmuir.1c01849
Langmuir 2021, 37, 12346−12355

parameters except the impact velocity. The sequential snapshots of the collision process for interaction intensity f = 0.6 are shown in Figure 3. Compared with the direct collision

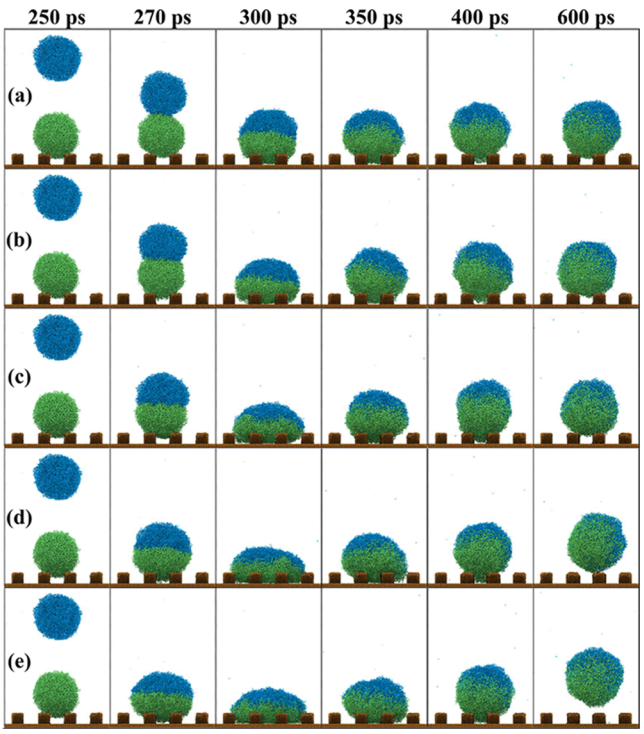

Figure 3. Snapshots of the collision processes of different impact velocities for interaction intensity f = 0.6 are shown at five moments. (a)−(e) Cases with impact velocities of 3, 4, 5, 6, and 7 Å/ps, respectively. The direction of the impact velocity is vertically downward.

of a droplet with the solid substrate, the situation studied in this paper has the collision and coalescence process between two droplets. Because the effect of air molecules can be ignored at this scale, a variety of phenomena in the macro-experimental research, including complete rebound and partial rebound with conglutination,[37] do not appear here. The collision process is divided into two stages: (i) In the coalescence and spreading stage, the upper droplet collides with the sessile droplet and two droplets coalesce directly. Meanwhile, the sessile droplet spreads out and penetrates into the structural gap of the substrate due to the action of inertial force. During the process of droplet deformation, a part of collision kinetic energy is converted into surface energy, and the other part is converted into internal energy due to viscous dissipation. (ii) In the retraction stage, the droplet that has become integrated retracts under the action of surface tension after reaching the maximum spreading state. When the interaction is strong enough, it is also possible that the coalescent droplets will not retract after spreading out, which is given in the follow-up research content.

To quantify the effects of impact velocity for the collision process, some crucial parameters are calculated and recorded. Since there is an initial distance between two droplets, the start moment t_{start} is defined as the moment when the centroidal velocity of the top droplet is less than V_0. Theoretically, the moment with the lowest droplet centroid height can be used as the maximum spreading moment, but we found that this could lead to miscalculation in practice, especially on surfaces with high interaction intensity. Refer to the method of Liu et al.,[44] the maximum spreading moment t_{max} is defined as the moment when there are most oxygen atoms under the contact layer and we can get the maximum spreading time $\tau = t_{max} - t_{start}$. The specific solution process is given in Section 1 of the Supporting Information. The parameters at different impact velocities are obtained by the same method. To obtain the spreading diameter of a droplet, the average density distribution shown in Figure 4a is calculated in a cylindrical coordinate system with the Z-axis passing through the centroid of the droplet and perpendicular to the surface.[24,43] The points near a density of 0.5 g/cm^3 are selected to determine the boundary, and the average diameter of the contact layer between the droplet and the upper surface of the solid is the spreading diameter (D_s) at this moment. Figure 4b shows the time evolution of the spreading factor β at different impact velocities. The variation process of β increasing initially and decreasing afterward corresponds to the two stages of droplet spreading and retraction. We can find that the subsequent value of β is almost constant at low impact velocity, which shows that the coalescent droplet is finally stable on the solid surface. But for high impact velocity, the value of β continuously decreases, which means that the coalescent droplet tends to detach from the surface and even bounces.

In addition, under the same surface and interaction intensity (model 1, f = 0.6), the relationship between the maximum speed factor β_{max} and the dimensionless maximum spread time

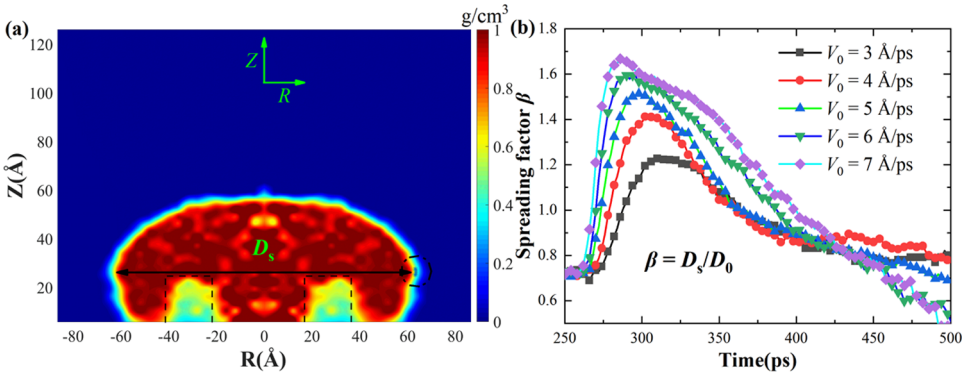

Figure 4. (a) Contour map of the average density distribution inside the coalescent droplet in circular cylindrical coordinates. The dotted line denotes the solid surface and the points within the circle represent the droplet boundaries at the contact layer. (b) Time evolution of the spreading factor β of the droplet at different impact velocities.

https://doi.org/10.1021/acs.langmuir.1c01849
Langmuir 2021, 37, 12346−12355

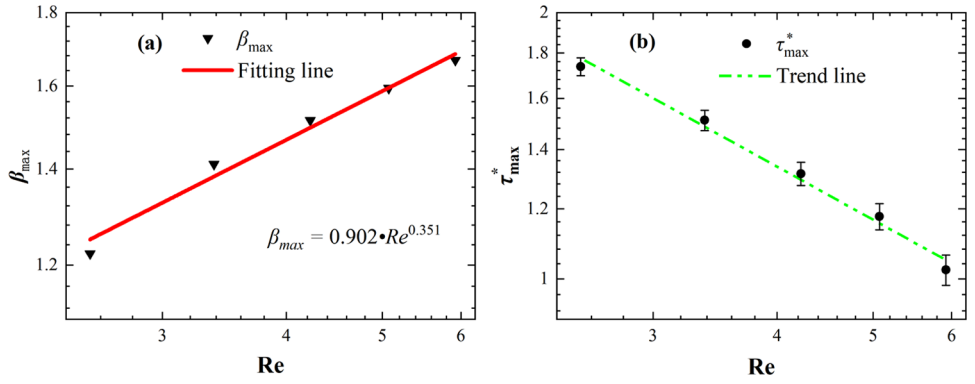

Figure 5. (a) Relationship between the maximum spreading factor β_{max} and the Reynolds number in the log−log coordinate. (b) The relationship between the dimensionless maximum spread time τ^*_{max} and the Reynolds number in the log−log coordinate.

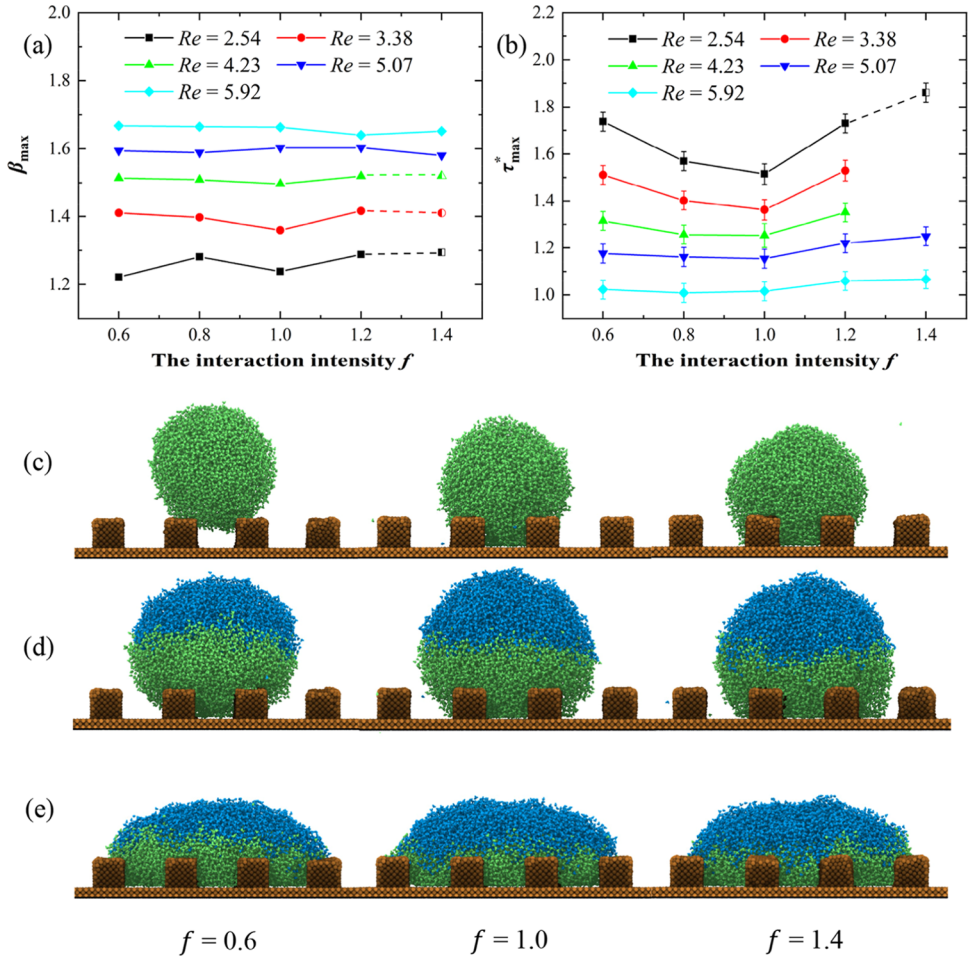

Figure 6. Collision process on model 1 with different f values. (a) The variation of β_{max} versus the Reynolds number and interaction intensity f. (b) The variation of τ^*_{max} versus the Reynolds number and interaction intensity f. The half-filled mark indicates that the droplet did not reach its maximum spreading state during the collision. (c) The initial wetting state of the sessile droplet. (d) The maximum spreading state for V_0 = 3 Å/ps. (e) The maximum spreading state for V_0 = 7 Å/ps.

τ^*_{max} and the Reynolds number is shown in Figure 5. The laws related to the Reynolds number or Weber number are equivalent since the Ohnesorge number $Oh = \sqrt{We}/Re$ only depends on the physical properties of the droplet and it is a fixed value in this study. Therefore, in the following discussion, we only choose the Reynolds number, and β_{max} is obtained by calculating the spreading factor at the maximum spreading moment t_{max}. Previous studies[45,46] have defined an inertial capillary time $\tau_0 = \sqrt{\rho D_0^3/8\sigma}$ that is only related to the physical properties of the droplet. To compare and eliminate the influence of size, we define the dimensionless maximum spreading time $\tau^*_{max} = \tau_{max}/\tau_0$. The results indicate that β_{max} increases as a power function trend with the Reynolds number, while τ^*_{max} decreases as a power function trend with the Reynolds number. This is the same as the results in the previous literature,[16,19] namely, β_{max} scales with Re^a and τ^*_{max}

https://doi.org/10.1021/acs.langmuir.1c01849
Langmuir 2021, 37, 12346−12355

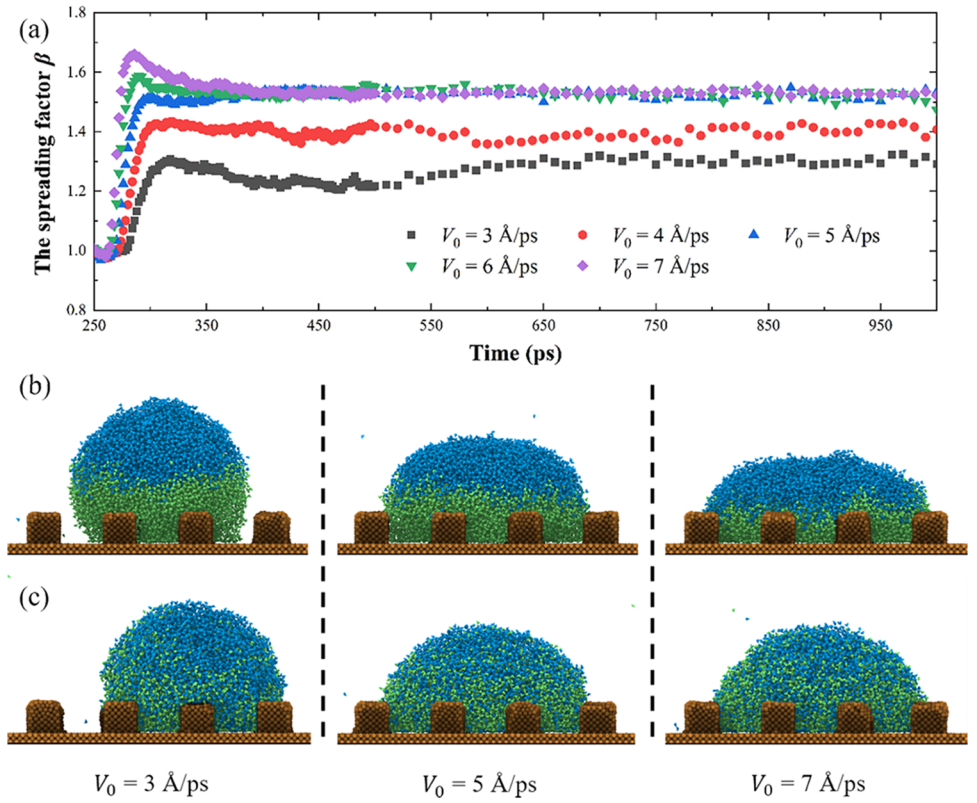

Figure 7. (a) Time evolution of the spreading factor β of the droplet at different impact velocities with interaction intensity f = 1.4 on model 1. (b) The maximum spreading state. (c) The stable spreading state.

scales with We^b from a simplified perspective. It indicates that the droplet spreading process follows a similar rule at the macroscopic and nanometer scales.

Effects of Surface Properties. The properties of a surface are mainly determined by two aspects, including the characteristics of nanostructures and the interaction intensity f. To study their respective effects on the head-on collision of double droplets, we first simulated the cases of model 1 with five different interaction intensities f, varying from 0.6 to 1.4. The variations of β_{max} and τ^*_{max} in different cases are shown in Figure 6. For different f values, the value of β_{max} is very close under the same Reynolds number, which means that the interaction intensity has less effect on the maximum spreading factor, especially in the range of larger impact velocity. As shown in Figure 6d,e, the spreading diameter on surfaces with different f values and the wetting state in the maximum spreading are approximately the same. This phenomenon occurs because most of the water molecules and surface atoms are close to each other in the coalescing and spreading stage, which shows the attraction effect. The interaction between these atoms consumes less kinetic energy of the collision, so the size of f has a relatively lesser influence on the maximum spreading factor. In addition, we found that for interaction intensity f = 1.4, the droplet may not reach the maximum spreading state during the collision process, which is shown as half-filled marks in Figure 6a,b. As shown in Figure 7a, when the impact velocity is 3−5 Å/ps, the maximum spreading factor of the droplet in the collision process is the same as that in the stable wetting state. It indicates that the droplet does not retract after spreading, and this is a special phenomenon when two droplets collide at a low velocity on a solid surface with strong interaction intensity. For V_0 = 3 Å/ps, such a change in the spreading factor curve is due to the droplet's movement on the surface, and the spreading factor in the stable state is basically the same as that in the collision spreading state. As shown in Figure 7b,c, comparing the stable spreading state with the maximum spreading state, droplet retraction is obvious at high impact velocity but not at low impact velocity.

For the maximum dimensionless spreading time τ^*_{max}, we find that the situation is different from β_{max}. In Figure 6b, it is observed that when $f \leq 1.0$, the value of τ^*_{max} decreases with the increase of f, but as the impact velocity increases, the extent of reduction becomes smaller and finally appears as a straight line, that is, the value of τ^*_{max} does not change with f at high impact velocity. Meanwhile, τ^*_{max} increases with the interaction intensity f when $f \geq 1.0$, and with the increase of collision velocity, the amplitude decreases. As shown in Figure 6, with the increase of interaction intensity, the wetting state of the sessile droplet changes from the Cassie state to the Wenzel state. This indicates that when f is less than 1.0, compared with the Cassie state, the sessile droplet in the Wenzel state is beneficial to reduce the time to reach the maximum spreading state. When f continues to increase after 1.0, although the sessile droplets are all in the Wenzel state, the strong solid−liquid interaction increases the time to reach the maximum spreading state. After analyzing the snapshots of the collision process, we find that in the cases of low impact velocity, the maximum spreading state of the droplet is mostly located outside the structural gap, showing a spherical shape, while at high impact velocity, it is in the shape of a pancake, mostly immersed in the structure gaps. This indicates that the wetting state of the droplet has an important effect on the maximum spreading time, especially at low impact velocity.

https://doi.org/10.1021/acs.langmuir.1c01849
Langmuir 2021, 37, 12346−12355

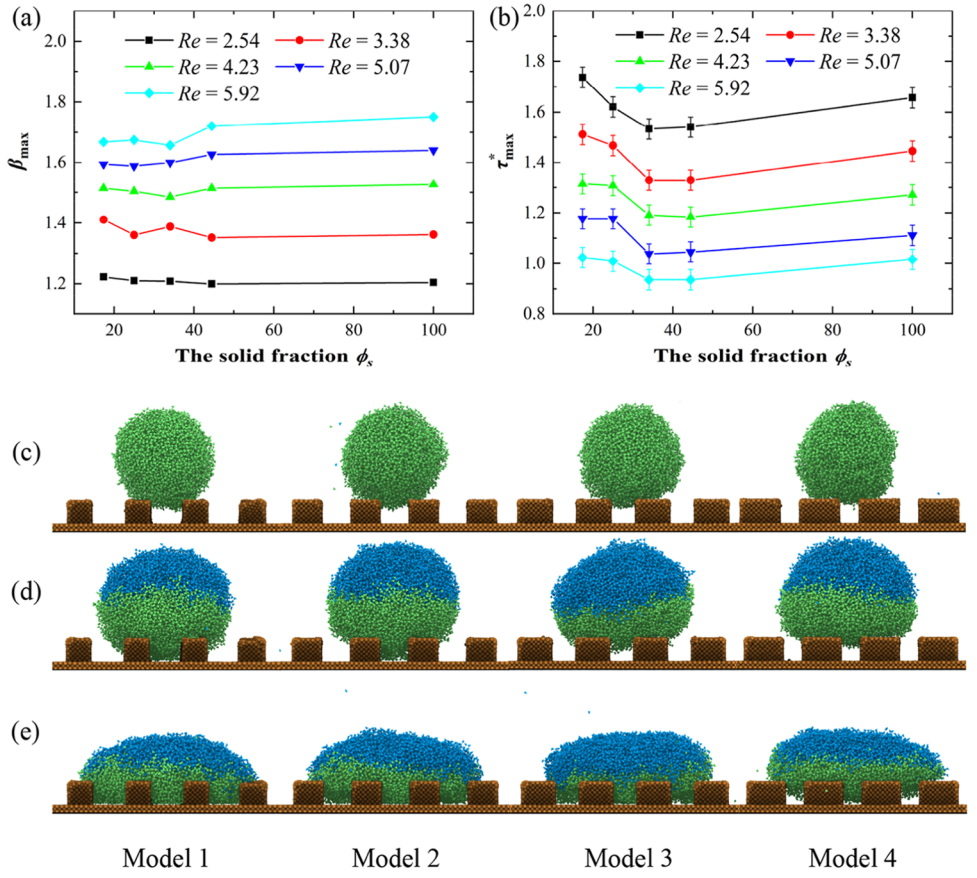

Figure 8. Collision process on different models with $f = 0.6$. (a) The variation of β_{max} versus the Reynolds number and the solid fraction. (b) The variation of τ^*_{max} versus the Reynolds number and the solid fraction. (c) The initial wetting state of a sessile droplet. (d) The maximum spreading state for $V_0 = 3$ Å/ps. (e) The maximum spreading state for $V_0 = 7$ Å/ps.

To study the effects of surface structure characteristics on the collision process, we simulate the head-on collision process of two droplets on five different models (Table 1) by keeping interaction intensity $f = 0.6$. Figure 8a shows the maximum spreading factor β_{max} under different solid fractions and Reynolds numbers. In general, at low impact velocity, β_{max} is basically a constant value on different solid fraction surfaces. As the impact velocity increases, the increasing trend of β_{max} with the solid fraction is more pronounced. Snapshots of the collision process show that the presence of a sessile droplet made it easier for the coalescent droplet to deform on its own rather than spread out on the surface at low impact velocity, so β_{max} is basically the same. The droplet spreads out sufficiently to show the effect of the surface structure in the range of high impact velocity. On the surface with a large solid fraction, the maximum spreading droplet is in the P−W state or even the Cassie state, which is beneficial to increase the maximum spreading factor. The relation between the dimensionless maximum spreading time τ^*_{max} and the Reynolds number on different solid fraction surfaces is shown in Figure 8b. As the solid fraction increases, τ^*_{max} first decreases and then increases. The value of τ^*_{max} on the smallest solid fraction surface and the smooth surface are located at both ends of a similar V-shaped curve. As shown in Figure 8, for the same impact velocity, from model 1 to model 3, the maximum spreading state of the coalescent droplet is in the Wenzel state, but the part of the droplet in the structural gap decreases gradually, which reduces the time to reach the maximum spreading. From model 3 to model 4, the maximum spreading state changes from the Wenzel state to the P−W state, and with the further increase of the solid fraction, it can be predicted that the maximum spreading state will eventually be the Cassie state. For the case where the maximum spreading state is the Wenzel state, the smaller the solid fraction, the more the droplets are immersed in the structural gap, the more obvious the blocking effect on the spreading of the droplets, and the longer the maximum spreading time. For the case where the maximum spreading state is the P−W or Cassie state, the larger the solid fraction, the larger the spreading range of the droplet on a solid surface, which will also lead to the increase of the maximum spreading time.

Theoretical Prediction of β_{max} on Model 5. By referring to the method used in the collision process of a single droplet with the surface, we give a theoretical prediction of the maximum spreading factor β_{max} of the collision process of two droplets on a smooth surface in model 5. The main idea is the conservation of energy in different states. The initial state energy of the upper droplet includes the kinetic energy $E_{k1} = \pi\rho D_0^3 V_0^2/12$ and the surface energy $E_{s1} = \pi D_0^2\sigma$. The initial kinetic energy of the sessile droplet is $E_{k2} = 0$. Assuming that the contact angle between the sessile droplet and the surface is θ, according to the conservation of volume, we can get the relationship between the wetting diameter of the sessile droplet D and the initial diameter D_0 on the hydrophobic surface.

$$D = A \cdot D_0 \tag{5}$$

https://doi.org/10.1021/acs.langmuir.1c01849
Langmuir 2021, 37, 12346−12355

$$A = \left(\frac{4}{4 - (1 + \cos\theta)^2(2 - \cos\theta)}\right)^{1/3} \quad (6)$$

So, we can get $E_{s2} = \pi D_0^2\sigma(1 - \cos\theta)A^2/2$. In the maximum spreading state, we suppose the droplet is a cylinder with a bottom diameter of D_{max} and a height of H, which can be calculated with volume conservation.

$$\frac{\pi D_{max}^2}{4}\cdot H = 2\cdot\frac{4\pi}{3}\left(\frac{D_0}{2}\right)^3 \quad (7)$$

$$H = \frac{4}{3}\left(\frac{D_0}{D_{max}}\right)^2 D_0 = \frac{4}{3}\left(\frac{1}{\beta_{max}}\right)^2 D_0 \quad (8)$$

It is very important to determine the viscous dissipation during droplet spreading. Here, we adopt the method proposed by Li et al.[34] in 2015. The dissipation energy during the collision process is calculated by

$$E_v = \int_{t_{start}}^{t_{max}}\int_{\Omega}\varphi\ \mathrm{d}\Omega\ \mathrm{d}t = \Omega\int_{t_{start}}^{t_{max}}\varphi\ \mathrm{d}t \quad (9)$$

$$\varphi = \mu\left(\frac{\partial v_i}{\partial x_j} + \frac{\partial v_j}{\partial x_i}\right)\frac{\partial v_i}{\partial x_j} \approx \mu\left(\frac{V_0}{h}\right)^2 \quad (10)$$

where t_{start} and t_{max} are the start moment and the maximum spreading moment of the collision process, Ω is the characteristic volume for viscous dissipation, and h is the characteristic height during the spreading process. Assuming the relationship between h and t is $\mathrm{d}h/\mathrm{d}t = -V_0$, and the boundary conditions are $h = \frac{D_0}{2}(2 + A - A\cos\theta)$ in t_{start} and $h = H$ in t_{max}. Combining the above equations we can get

$$E_v = \frac{1}{4}\pi\mu D_0^2 V_0\left(\beta_{max}^2 - \frac{8}{3(2 + A - A\cos\theta)}\right) \quad (11)$$

In the maximum spreading state of the droplet, the kinetic energy is $E_k = 0$ and the surface energy $E_s = (\pi D_{max}^2/4 + \pi D_{max}H)\sigma$. The change of interfacial energy between the droplet and the solid surface is ignored. According to the energy conservation equation: $E_{k1} + E_{k2} + E_{s1} + E_{s2} = E_k + E_s + E_v$, we can get

$$\left(1 + \frac{We}{Re}\right)\beta_{max}^3 - \left(\frac{We}{3} + 4 + 2(1 - \cos\theta)A^2 + \frac{8}{3(2 + A - A\cos\theta)}\frac{We}{Re}\right)\beta_{max} + \frac{16}{3} = 0 \quad (12)$$

where θ is the initial contact angle of the droplet, and A is the diameter increase coefficient after the initial droplet spreads on the surface, which is shown in eq 6. Substituting the corresponding parameters of different impacting velocities into eq 12 and solving it, we can get theoretical maximum spreading factors. The parameters of different impacting velocities on model 5 with interaction intensity $f = 0.6$ are shown in Table 4.

Figure 9 shows the variation of β_{max} versus the Reynolds number in different theoretical models. Compared to the previous model for a single nanodroplet impacting the surface, our theoretical predictions of β_{max} are in good agreement with the MD results, which means that the head-on collision process of two nanodroplets needs a unique prediction model. In this paper, we just make a theoretical prediction of the process on a smooth surface, and the collision process on a complex rough structure surface needs further study.

Table 4. Parameters of Different Impacting Velocities on Model 5 with Interaction Intensity $f = 0.6$[a]

V_0 (Å/ps)	3	4	5	6	7
Re	2.54	3.38	4.23	5.07	5.92
initial contact angle θ (deg)	131	131	131	131	131
spreading contact angle θ_s (deg)	146	141	143	140	151
maximum spreading factor β_{max}	1.204	1.362	1.526	1.640	1.751
theoretical prediction	1.425	1.480	1.548	1.619	1.692
absolute relative errors (%)	18.3	8.7	1.4	1.3	3.3

[a]The initial contact angle is the contact of the sessile droplet. The spreading contact angle is the contact angle of the droplet in the maximum spreading state, which is used in the modified model of Li et al.[34]

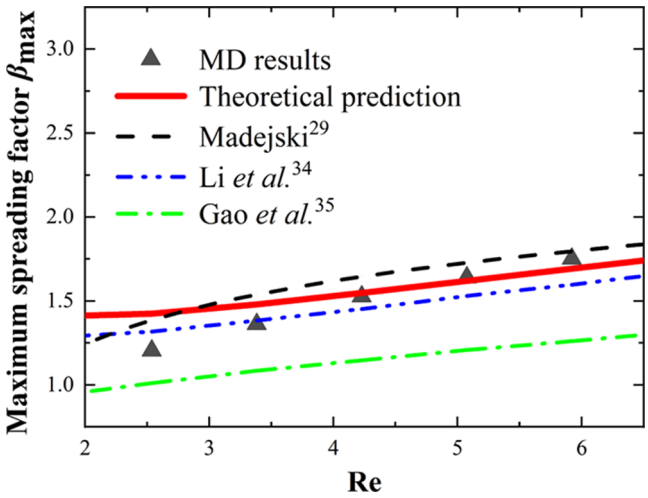

Figure 9. Comparison of β_{max} among the MD results, theoretical predictions, and previous models.

CONCLUSIONS

A head-on collision process of two nanodroplets on a solid surface was studied using the molecular dynamics simulation method. The maximum spreading factor β_{max} and the dimensionless maximum spreading time τ_{max}^* were calculated and analyzed to describe the collision process. The MD simulation results on the same surface show that β_{max} increases as a power function trend with the Reynolds number, while τ_{max}^* decreases as a power function trend with the Reynolds number, which is consistent with macroscopic experimental results. In addition, we find that among the two factors that affect the properties of the nanoscale surface, the interaction intensity f has less effect on β_{max} since it does not fundamentally change the wetting state of the droplet at its maximum spreading state. When $f \le 1.0$, it reduces the maximum dimensionless spreading time τ_{max}^* by changing the initial wetting state of the sessile droplet, and when $f \ge 1.0$, it enlarges τ_{max}^* by enhancing the wettability between the droplet and structure gaps, while the initial wetting state of the sessile droplet is the same. With the increase of impact velocity, both

https://doi.org/10.1021/acs.langmuir.1c01849
Langmuir 2021, 37, 12346−12355

the effects of the interaction intensity f decrease. For different surface structure models, the simulation results indicate that β_{max} is basically a constant value on different solid fraction surfaces at low impact velocity. As the impact velocity increases, the increasing trend of β_{max} with the solid fraction is more pronounced since the droplet can be fully spread at this time. As the solid fraction increases, τ^*_{max} first decreases and then increases. The maximum spreading state of the coalescent droplet from the Wenzel state to the Cassie state is beneficial to decrease τ^*_{max}, but the increase of the solid fraction after reaching the Cassie state will increase β_{max} and τ^*_{max}. This shows that adjusting interaction intensity and the solid fraction to make the sessile droplet approach the Wenzel state and the coalescent droplet approach the Cassie state might make the collision process of the double droplet achieve greater spreading in a shorter time. At last, we established a theoretical model to predict β_{max} of a head-on collision of two nanodroplets on a smooth surface, which shows good accuracy, especially in the range of high impact velocity.

■ ASSOCIATED CONTENT

Supporting Information

The Supporting Information is available free of charge at https://pubs.acs.org/doi/10.1021/acs.langmuir.1c01849.

Calculation method of the maximum spreading time; definition of the contact layer; initial contact angle; and additional snapshots of the collision process (PDF)

■ AUTHOR INFORMATION

Corresponding Authors

Wei Liu − *School of Energy and Power Engineering, Huazhong University of Science and Technology, Wuhan 430074, China*; Email: w_liu@hust.edu.cn

Zhichun Liu − *School of Energy and Power Engineering, Huazhong University of Science and Technology, Wuhan 430074, China*; orcid.org/0000-0001-9645-3052; Email: zcliu@hust.edu.cn

Authors

Peng Mao − *School of Energy and Power Engineering, Huazhong University of Science and Technology, Wuhan 430074, China*; orcid.org/0000-0002-3746-7937

Shan Gao − *School of Energy and Power Engineering, Huazhong University of Science and Technology, Wuhan 430074, China; School of Energy and Power Engineering, Jiangsu University, Zhenjiang 212013, China*

Complete contact information is available at: https://pubs.acs.org/10.1021/acs.langmuir.1c01849

Notes

The authors declare no competing financial interest.

■ ACKNOWLEDGMENTS

This project was supported by the National Natural Science Foundation of China (Nos. 51736004 and 51776079). The study was performed at the National Supercomputer Center in Tianjin, and the calculations were performed on TianHe-1(A).

■ REFERENCES

(1) Tuteja, A.; Choi, W.; Ma, M.; Mabry, J. M.; Mazzella, S. A.; Rutledge, G. C.; McKinley, G. H.; Cohen, R. E. Designing superoleophobic surfaces. *Science* **2007**, *318*, 1618−1622.

(2) Deng, X.; Mammen, L.; Butt, H. J.; Vollmer, D. Candle soot as a template for a transparent robust superamphiphobic coating. *Science* **2012**, *335*, 67−70.

(3) Blossey, R. Self-cleaning surfaces–virtual realities. *Nat. Mater.* **2003**, *2*, 301−306.

(4) Wen, R.; Xu, S.; Ma, X.; Lee, Y.-C.; Yang, R. Three-Dimensional Superhydrophobic Nanowire Networks for Enhancing Condensation Heat Transfer. *Joule* **2018**, *2*, 269−279.

(5) Liu, Y.; Moevius, L.; Xu, X.; Qian, T.; Yeomans, J. M.; Wang, Z. Pancake bouncing on superhydrophobic surfaces. *Nat. Phys.* **2014**, *10*, 515−519.

(6) Hao, C.; Liu, Y.; Chen, X.; Li, J.; Zhang, M.; Zhao, Y.; Wang, Z. Bioinspired Interfacial Materials with Enhanced Drop Mobility: From Fundamentals to Multifunctional Applications. *Small* **2016**, *12*, 1825−1839.

(7) Galliker, P.; Schneider, J.; Eghlidi, H.; Kress, S.; Sandoghdar, V.; Poulikakos, D. Direct printing of nanostructures by electrostatic autofocussing of ink nanodroplets. *Nat. Commun.* **2012**, *3*, No. 890.

(8) Chen, X.; Wu, J.; Ma, R.; Hua, M.; Koratkar, N.; Yao, S.; Wang, Z. Nanograssed Micropyramidal Architectures for Continuous Dropwise Condensation. *Adv. Funct. Mater.* **2011**, *21*, 4617−4623.

(9) Jung, S.; Tiwari, M. K.; Doan, N. V.; Poulikakos, D. Mechanism of supercooled droplet freezing on surfaces. *Nat. Commun.* **2012**, *3*, No. 615.

(10) Stone, H. A. Ice-phobic surfaces that are wet. *ACS Nano* **2012**, *6*, 6536−6540.

(11) Mishchenko, L.; Hatton, B.; Bahadur, V.; Taylor, J. A.; Krupenkin, T.; Aizenberg, J. Design of ice-free nanostructured surfaces based on repulsion of impacting water droplets. *ACS Nano* **2010**, *4*, 7699−7707.

(12) Huang, H.-M.; Chen, X.-P. Energetic analysis of drop's maximum spreading on solid surface with low impact speed. *Phys. Fluids* **2018**, *30*, No. 022106.

(13) Jung, S.; Hutchings, I. M. The impact and spreading of a small liquid drop on a non-porous substrate over an extended time scale. *Soft Matter* **2012**, *8*, 2686−2696.

(14) Mertaniemi, H.; Forchheimer, R.; Ikkala, O.; Ras, R. H. Rebounding droplet-droplet collisions on superhydrophobic surfaces: from the phenomenon to droplet logic. *Adv. Mater.* **2012**, *24*, 5738−5743.

(15) Kim, H.; Lee, C.; Kim, M. H.; Kim, J. Drop impact characteristics and structure effects of hydrophobic surfaces with micro- and/or nanoscaled structures. *Langmuir* **2012**, *28*, 11250−11257.

(16) Lin, S.; Zhao, B.; Zou, S.; Guo, J.; Wei, Z.; Chen, L. Impact of viscous droplets on different wettable surfaces: Impact phenomena, the maximum spreading factor, spreading time and post-impact oscillation. *J. Colloid Interface Sci.* **2018**, *516*, 86−97.

(17) Zhao, B.; Wang, X.; Zhang, K.; Chen, L.; Deng, X. Impact of Viscous Droplets on Superamphiphobic Surfaces. *Langmuir* **2017**, *33*, 144−151.

(18) Vadillo, D. C.; Soucemarianadin, A.; Delattre, C.; Roux, D. C. D. Dynamic contact angle effects onto the maximum drop impact spreading on solid surfaces. *Phys. Fluids* **2009**, *21*, No. 122002.

(19) Lee, J. B.; Derome, D.; Guyer, R.; Carmeliet, J. Modeling the Maximum Spreading of Liquid Droplets Impacting Wetting and Nonwetting Surfaces. *Langmuir* **2016**, *32*, 1299−1308.

(20) Lee, J. B.; Lee, S. H. Dynamic wetting and spreading characteristics of a liquid droplet impinging on hydrophobic textured surfaces. *Langmuir* **2011**, *27*, 6565−6573.

(21) Guo, L.; Tang, G. H.; Kumar, S. Dynamic Wettability on the Lubricant-Impregnated Surface: From Nucleation to Growth and Coalescence. *ACS Appl. Mater. Interfaces* **2020**, *12*, 26555−26565.

(22) Castrejon-Pita, J. R.; Betton, E. S.; Kubiak, K. J.; Wilson, M. C.; Hutchings, I. M. The dynamics of the impact and coalescence of droplets on a solid surface. *Biomicrofluidics* **2011**, *5*, No. 014112.

(23) Li, H.; Zhang, K. Dynamic behavior of water droplets impacting on the superhydrophobic surface: Both experimental study and

molecular dynamics simulation study. *Appl. Surf. Sci.* **2019**, *498*, No. 143793.
(24) Gao, S.; Liao, Q.; Liu, W.; Liu, Z. Effects of Solid Fraction on Droplet Wetting and Vapor Condensation: A Molecular Dynamic Simulation Study. *Langmuir* **2017**, *33*, 12379−12388.
(25) Bordbar, A.; Taassob, A.; Khojasteh, D.; Marengo, M.; Kamali, R. Maximum Spreading and Rebound of a Droplet Impacting onto a Spherical Surface at Low Weber Numbers. *Langmuir* **2018**, *34*, 5149−5158.
(26) Wang, Y. B.; Wang, Y. F.; Gao, S. R.; Yang, Y. R.; Wang, X. D.; Chen, M. Universal Model for the Maximum Spreading Factor of Impacting Nanodroplets: From Hydrophilic to Hydrophobic Surfaces. *Langmuir* **2020**, *36*, 9306−9316.
(27) Wang, Y.-F.; Wang, Y.-B.; Xie, F.-F.; Liu, J.-Y.; Wang, S.-L.; Yang, Y.-R.; Gao, S.-R.; Wang, X.-D. Spreading and retraction kinetics for impact of nanodroplets on hydrophobic surfaces. *Phys. Fluids* **2020**, *32*, No. 092005.
(28) Pasandideh-Fard, M.; Qiao, Y. M.; Chandra, S.; Mostaghimi, J. Capillary effects during droplet impact on a solid surface. *Phys. Fluids* **1996**, *8*, 650−659.
(29) Madejski, J. Solidification of droplets on a cold surface. *Int. J. Heat Mass Transfer* **1976**, *19*, 1009−1013.
(30) Xie, F. F.; Lv, S. H.; Yang, Y. R.; Wang, X. D. Contact Time of a Bouncing Nanodroplet. *J. Phys. Chem. Lett.* **2020**, *11*, 2818−2823.
(31) Niu, D.; Tang, G. H. The effect of surface wettability on water vapor condensation in nanoscale. *Sci. Rep.* **2016**, *6*, No. 19192.
(32) Guo, L.; Tang, G. H.; Kumar, S. Droplet Morphology and Mobility on Lubricant-Impregnated Surfaces: A Molecular Dynamics Study. *Langmuir* **2019**, *35*, 16377−16387.
(33) Li, B.-X.; Li, X.-H.; Chen, M. Spreading and breakup of nanodroplet impinging on surface. *Phys. Fluids* **2017**, *29*, No. 012003.
(34) Li, X.-H.; Zhang, X.-X.; Chen, M. Estimation of viscous dissipation in nanodroplet impact and spreading. *Phys. Fluids* **2015**, *27*, No. 052007.
(35) Gao, S.; Liao, Q.; Liu, W.; Liu, Z. Nanodroplets Impact on Rough Surfaces: A Simulation and Theoretical Study. *Langmuir* **2018**, *34*, 5910−5917.
(36) Rayleigh, L. XIII. Further observations upon liquid jets, in continuation of those recorded in the Royal Society's 'Proceedings' for March and May, 1879. In *Proceedings of the Royal Society of London*, 1883; pp 130−145.
(37) Wang, F. C.; Feng, J. T.; Zhao, Y. P. The head-on colliding process of binary liquid droplets at low velocity: high-speed photography experiments and modeling. *J. Colloid Interface Sci.* **2008**, *326*, 196−200.
(38) Graham, P. J.; Farhangi, M. M.; Dolatabadi, A. Dynamics of droplet coalescence in response to increasing hydrophobicity. *Phys. Fluids* **2012**, *24*, No. 112105.
(39) Plimpton, S. Fast parallel algorithms for short-range molecular dynamics. *J. Comput. Phys.* **1995**, *117*, 1−19.
(40) Stukowski, A. Visualization and analysis of atomistic simulation data with OVITO−the Open Visualization Tool. *Modell. Simul. Mater. Sci. Eng.* **2009**, *18*, No. 015012.
(41) Soper, A.; Phillips, M. A new determination of the structure of water at 25 C. *Chem. Phys.* **1986**, *107*, 47−60.
(42) Soper, A.; Bruni, F.; Ricci, M. Site−site pair correlation functions of water from 25 to 400 C: Revised analysis of new and old diffraction data. *J. Chem. Phys.* **1997**, *106*, 247−254.
(43) Huang, C.; Xu, F.; Sun, Y. Effects of morphology, tension and vibration on wettability of graphene: A molecular dynamics study. *Comput. Mater. Sci.* **2017**, *139*, 216−224.
(44) Liu, H.; Chu, F.; Zhang, J.; Wen, D. Nanodroplets impact on surfaces decorated with ridges. *Phys. Rev. Fluids* **2020**, *5*, No. 074201.
(45) Richard, D.; Clanet, C.; Quéré, D. Surface phenomena: Contact time of a bouncing drop. *Nature* **2002**, *417*, 811.
(46) Bird, J. C.; Dhiman, R.; Kwon, H. M.; Varanasi, K. K. Reducing the contact time of a bouncing drop. *Nature* **2013**, *503*, 385−388.

https://doi.org/10.1021/acs.langmuir.1c01849
Langmuir 2021, 37, 12346−12355